



HAL
open science

Atomic layer deposition of $\text{La}_x\text{Zr}_{1-x}\text{O}_2$ ($x=0.25$) high-k dielectrics for advanced gate stacks

D. Tsoutsou, L. Lamagna, S. N. Volkos, A. Molle, S. Baldovino, Sylvie Schamm-Chardon, Pierre-Eugène Coulon, M. Fanciulli

► **To cite this version:**

D. Tsoutsou, L. Lamagna, S. N. Volkos, A. Molle, S. Baldovino, et al.. Atomic layer deposition of $\text{La}_x\text{Zr}_{1-x}\text{O}_2$ ($x=0.25$) high-k dielectrics for advanced gate stacks. Applied Physics Letters, 2009, 94 (5), pp.53504 - 53504. 10.1063/1.3075609 . hal-01745031

HAL Id: hal-01745031

<https://hal.science/hal-01745031>

Submitted on 9 Apr 2018

HAL is a multi-disciplinary open access archive for the deposit and dissemination of scientific research documents, whether they are published or not. The documents may come from teaching and research institutions in France or abroad, or from public or private research centers.

L'archive ouverte pluridisciplinaire **HAL**, est destinée au dépôt et à la diffusion de documents scientifiques de niveau recherche, publiés ou non, émanant des établissements d'enseignement et de recherche français ou étrangers, des laboratoires publics ou privés.

Atomic layer deposition of $\text{La}_x\text{Zr}_{1-x}\text{O}_{2-\delta}$ ($x = 0.25$) high- k dielectrics for advanced gate stacks

D. Tsoutsou, L. Lamagna, S. N. Volkos, A. Molle, S. Baldovino, S. Schamm, P. E. Coulon, and M. Fanciulli

Citation: *Appl. Phys. Lett.* **94**, 053504 (2009); doi: 10.1063/1.3075609

View online: <https://doi.org/10.1063/1.3075609>

View Table of Contents: <http://aip.scitation.org/toc/apl/94/5>

Published by the [American Institute of Physics](#)

Articles you may be interested in

[Structural and electrical properties of atomic layer deposited Al-doped \$\text{ZrO}_2\$ films and of the interface with TaN electrode](#)

Journal of Applied Physics **112**, 014107 (2012); 10.1063/1.4731746

[Stabilization of very high- \$k\$ tetragonal phase in Ge-doped \$\text{ZrO}_2\$ films grown by atomic oxygen beam deposition](#)

Journal of Applied Physics **106**, 024107 (2009); 10.1063/1.3182636

[High- \$\kappa\$ gate dielectrics: Current status and materials properties considerations](#)

Journal of Applied Physics **89**, 5243 (2001); 10.1063/1.1361065



Scilight

Sharp, quick summaries **illuminating**
the latest physics research

Sign up for **FREE!**

AIP
Publishing

Atomic layer deposition of $\text{La}_x\text{Zr}_{1-x}\text{O}_{2-\delta}$ ($x=0.25$) high- k dielectrics for advanced gate stacks

D. Tsoutsou,¹ L. Lamagna,^{1,a)} S. N. Volkos,¹ A. Molle,¹ S. Baldovino,¹ S. Schamm,² P. E. Coulon,² and M. Fanciulli^{1,3}

¹Laboratorio Nazionale MDM, CNR-INFN, Via C. Olivetti 2, Agrate Brianza (MI) 20041, Italy

²CEMES-CNRS, Université de Toulouse, 29 rue J. Marvig, BP 94347, 31055 Toulouse Cedex 4, France

³Dipartimento di Scienza dei Materiali, Università degli studi di Milano-Bicocca, Milano, Italy

(Received 16 September 2008; accepted 22 December 2008; published online 3 February 2009)

Thin $\text{La}_x\text{Zr}_{1-x}\text{O}_{2-\delta}$ ($x=0.25$) high permittivity (k) films are grown on Si(100) by atomic layer deposition at 300 °C using $(^1\text{PrCp})_3\text{La}$, $(\text{MeCp})_2\text{ZrMe}(\text{OMe})$ and O_3 species. Their properties are studied by grazing incidence x-ray diffraction, high resolution transmission electron microscopy, electron energy loss spectroscopy, x-ray photoelectron spectroscopy, and electrical measurements on the as-grown films and after vacuum annealing at 600 °C. Annealed films feature resistance to hygroscopicity, a large k value of around 30 and an acceptable leakage current density. A low- k silica-rich interlayer is also evidenced at both pristine and annealed high- k /Si interfaces. © 2009 American Institute of Physics. [DOI: 10.1063/1.3075609]

As the complementary metal oxide semiconductor (CMOS) device dimensions continue to decrease in order to improve chip performance, high permittivity (high- k) oxides are being introduced into the CMOS technology as alternative dielectrics to SiO_xN_y with the principal aim to suppress detrimental gate leakage current effects.¹ Among the various rare earth oxides² currently considered for the sub-45 nm high- k CMOS era is La_2O_3 mainly due to its high k value (~ 27 when crystallized into the hexagonal $P6_3/mmc$ phase)³ and wide band gap energy (~ 6 eV).⁴ However, $\text{La}(\text{OH})_3$ formation due to OH^- groups absorption when La_2O_3 is exposed to air significantly degrades its k value.⁵ ZrO_2 could be another option for the sub-45 nm high- k CMOS nodes because it satisfies technology requirements in terms of k value and band gap energy but the material is marginally chemically/thermally stable on Si,⁶ therefore, restricting an aggressive scaling down of the equivalent oxide thickness (EOT). Alloying ZrO_2 with La_2O_3 to produce a ternary $\text{La}_x\text{Zr}_{1-x}\text{O}_{2-\delta}$ (LZO) compound might be a promising route to engineer a material suitable for high- k dielectric applications. Among the various LZO growth techniques,^{7–12} atomic layer deposition (ALD) appears to be the most attractive one for integration into the CMOS flow as it provides the capability to grow smooth and conformal films at low temperatures, allowing an accurate film thickness control.¹³

In this article, we report on the growth of LZO/Si interfaces by ALD using O_3 , a more powerful oxidizer than H_2O tested by Gaskell *et al.*,^{10,12} in combination with the same La [i.e., $(^1\text{PrCp})_3\text{La}$] and Zr [i.e., $(\text{MeCp})_2\text{ZrMe}(\text{OMe})$]; also known as ZrD-04] precursors as in Refs. 10 and 12. Contrary to Refs. 10–12, which are almost exclusively concerned with the properties of as-grown LZO films, our study merely focuses on annealed films since CMOS device processing involves postdeposition thermal treatments. LZO films were deposited in the Savannah 200 (Cambridge Nanotech Inc.) ALD reactor on H-terminated n -Si(100) at a growth temperature of 300 °C. $(^1\text{PrCp})_3\text{La}$ and ZrD-04 complexes were

kept at 150 and 110 °C, respectively. O_3 was injected into the reactor at a concentration ~ 200 g/Nm³. ALD cycle number varied between 12 and 50, resulting in a stack thickness within the 5–30 nm range. La atomic fraction $x = \text{La}/(\text{La}+\text{Zr})=0.25$, which was tuned by altering the ALD pulse number in the growth cycle, was estimated from the La 3d and Zr 3d core-level x-ray photoelectron spectroscopy (XPS) lines relying on the relevant atomic sensitivity factors. Postgrowth rapid thermal annealing (RTA) was performed for 60 s in vacuum (~ 1 mbar) at 600 °C. As opposed to RTA in forming gas or N_2 , annealing in vacuum permits monitoring of thermally induced structural, compositional, and electrical changes minimizing any contribution to them from the ambient. Moreover, vacuum should enhance the removal of the OH^- groups from the La-based film.

LZO films were characterized by a combination of (i) grazing incidence x-ray diffraction (GIXRD), (ii) transmission electron microscopy in the high resolution (HRTEM) and electron energy loss spectroscopy (EELS) modes, (iii) XPS, (iv) capacitance-voltage (C - V), parallel conductance-voltage (G_p - V) and current density-voltage (J - V) measurements. GIXRD spectra were collected with a position sensitive detector using the $\text{Cu } K\alpha$ radiation. The local structural and chemical properties around the film/substrate interface and in the film were analyzed by HRTEM and EELS with a field emission transmission electron microscope (FEI Tecnai™ F20) operated at 200 kV, equipped with a spherical aberration corrector and, for local EELS studies, with a scanning stage (STEM) and an imaging filter (Gatan GIF TRIDIEM). Cross-sectional TEM samples (bulk is cut perpendicular to the film/substrate interface) were prepared by classical procedures. XPS spectra were recorded at a take-off angle of 90° in a semispherical spectrometer employing a standard Al $K\alpha$ source (1486.6 eV) with an energy resolution of 0.8 eV and a pass energy of 20 eV. A multiple function fit was applied to the XPS data. Briefly, a Shirley baseline was removed from each XPS spectrum and all the Si oxidation state contributions were then fitted by single Gaussian-Lorentzian functions. Room temperature electrical measurements were performed on metal insulator semiconductor

^{a)} Author to whom correspondence should be addressed. Electronic mail: luca.lamagna@mdm.infn.it.

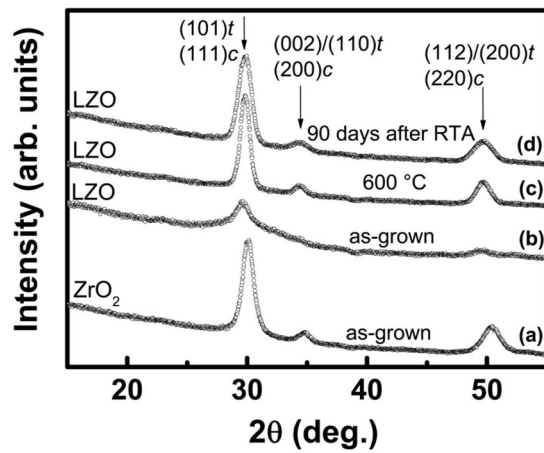


FIG. 1. GIXRD spectra for the 24 nm ZrO_2 and LZO films. Incidence angle was 1° and angular resolution was 0.03° .

(MIS) capacitors of $7.8 \times 10^{-4} \text{ cm}^2$ area. Capacitance equivalent oxide thickness (CET) was determined from the device accumulation capacitance at 800 kHz.

Figure 1 displays GIXRD spectra for the 24 nm thick ZrO_2 and LZO films. Although the monoclinic phase is the most stable phase¹⁴ for pure ZrO_2 below 1100°C , the as-grown ZrO_2 film [Fig. 1(a)], which was deposited at 300°C using the ZrD-04 and O_3 recipe,¹⁵ is found to adopt a cubic (*c*-) or tetragonal (*t*-) ZrO_2 structure¹⁶ owing to ALD growth under nonequilibrium conditions. An XRD-based delineation between the *c*- and *t*- ZrO_2 phases is difficult since the respective reflections¹⁶ appear at vicinal angles. La incorporation into the host ZrO_2 matrix through the ternary ALD process mostly generates thin amorphous as-grown LZO films as evidenced from the low signal in Fig. 1(b) and subsequently confirmed by the TEM image in Fig. 2(a). As illustrated in Fig. 1(c), LZO films crystallize after RTA into the *c*- or *t*- ZrO_2 phases. Thinner (20 and 12 nm) LZO films were found (data not shown) to exhibit the same structural behavior as the 24 nm thick one. Contrary to La_2O_3 films, LZO films are not hygroscopic as demonstrated by both Fig. 1(d)

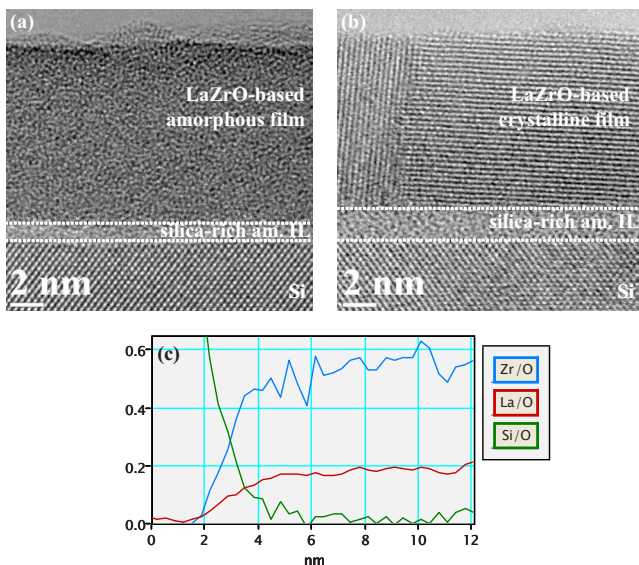


FIG. 2. (Color online) Cross-section HRTEM images for the 12 nm thick LZO film. (a) As-grown state. (b) After RTA for 60 s in vacuum at 600°C . Dotted lines are guide to the eye. (c) STEM-EELS profiles of elemental La/O , Zr/O , and Si/O ratios for the annealed state.

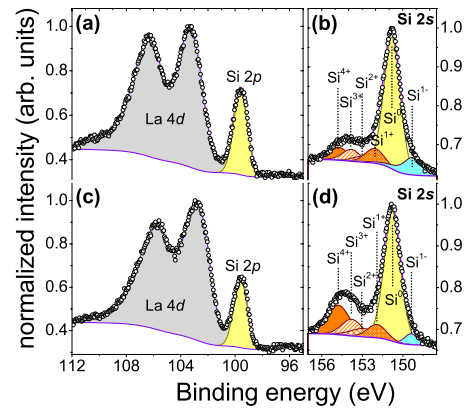


FIG. 3. (Color online) XPS Si $2p$ and $2s$ shape profiles at a take-off angle of 90° for a 5 nm thick LZO film. [(a)–(b)] Si $2p$ and $2s$ lines for the as-grown state. [(c)–(d)] Si $2p$ and $2s$ lines after RTA for 60 s in vacuum at 600°C . Chemical shifts are 1.3, 2.1, 3.1, and 4.0 eV for $1+$, $2+$, $3+$, and $4+$ oxidation states, respectively.

and XPS O $1s$ line (data not shown) taken after 90 days long exposure to air.

HRTEM data were recorded on the 12 nm thick as-grown and annealed LZO stacks. As depicted in Figs. 2(a) and 2(b), an amorphous interface layer (IL) of clear contrast, which suggests a silica-rich nature, appears just above the Si substrate for both cases with the IL thickness increasing after RTA. Atop the IL, a predominantly amorphous high-*k* layer for the as-grown stack and a crystalline one for the annealed stack are observed. Crystallographic parameters measured on the projected planes of the HRTEM images and on selected area electron diffraction patterns (data not shown) correspond to those for the *c*- or *t*- ZrO_2 phases.¹⁶ From the EELS spectra collected across the film/substrate interface towards the film and encompassing characteristic La, O, and Si ionization edges, the relative elemental La/O, Zr/O, and Si/O ratios were extracted and plotted as a function of the distance from the Si surface. For the annealed stack, Fig. 2(c) displays that past a Si- and O-rich near-interface region, the La/O and Zr/O ratios remain fairly constant not only along the film thickness but also in the direction parallel to the film/substrate interface. Differently from Ref. 11, no cluster nucleation, as revealed by TEM-EELS analysis, occurs at the interface or in the film.

To unveil the IL composition, an XPS analysis was conducted on a 5 nm thick LZO stack. Since the La $4d$ line overlaps with the high binding energy (BE) tail of the Si $2p$ line, we considered the Si $2s$ line for the pertinent analysis. Figure 3 compares the Si $2s$ lines for the as-grown and annealed stacks. The Si $2s$ peak is decomposed into six components: elemental Si (Si^0), four oxidation state components (Si^{1+} , Si^{2+} , Si^{3+} , and Si^{4+} corresponding to Si_2O , SiO , Si_2O_3 , and SiO_2 species, respectively),¹⁷ and an additional component (Si^{1-}) related to a minor Si-metal bonding. In agreement with HRTEM analysis, XPS data manifest a RTA-induced increase in the IL thickness because the broad peak due to the overall oxide contribution is larger after RTA. They also corroborate the STEM-EELS data on the silica-rich nature of the IL since the Si^{4+} component, which implies a SiO_2 bonding arrangement, dominates after RTA.

Figure 4(a) illustrates *C-V* curves for as-grown and annealed 13 nm thick LZO stacks. For both cases, accumulation capacitance exhibits minor frequency dispersion within

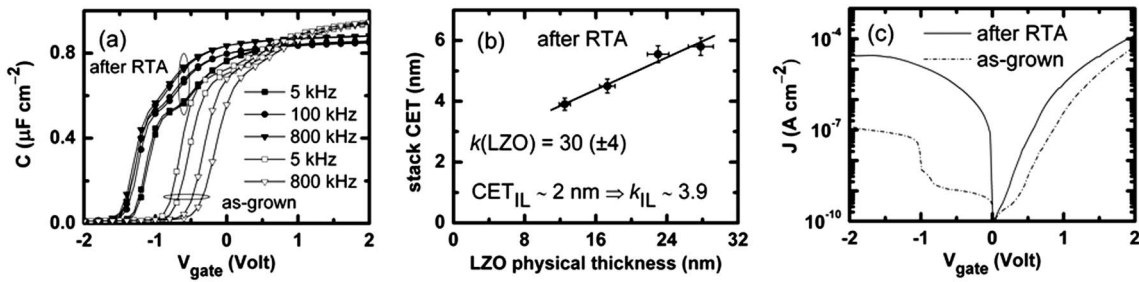


FIG. 4. Electrical characteristics for Al-gate MIS capacitors from a 13 nm thick LZO stack. (a) Multifrequency C - V curves for as-grown (empty symbols) and RTA-treated (filled symbols) devices. (b) Stack CET vs LZO film physical thickness plot for RTA-treated devices. (c) J - V curves for as-grown and RTA-treated devices. RTA was carried out for 60 s in vacuum at 600 °C. MIS capacitors received no postmetallization annealing.

the 5–800 kHz range. Table I summarizes electrical figures of merit derived from the data of Fig. 4(a). Evidently, RTA notably lowers the density of oxide trapped charge and interface defects (D_{it}) while markedly enhancing the positive fixed charge density near the dielectric/Si interface. From the slope of a linear fit to a stack CET versus LZO physical thickness plot in Fig. 4(b), the k value for annealed LZO films is estimated to be ~ 30 . Based on the theoretically calculated k value for different ZrO_2 crystalline phases,^{14,20} our result points more to a c - rather than t - ZrO_2 phases. In good agreement with the HRTEM and STEM-EELS analyses, the fit to the above plot intercepts with the y -axis at a point corresponding to an IL with a k value close to that of SiO_2 . Our as-grown LZO films feature a k value that varies with the stack thickness such that it is as low as 17.5 for a 12.5 nm thick stack and as high as 24 for a 22.5 nm thick stack. In the light of dark field TEM images (data not shown), this trend is ascribed to the fact that as-grown LZO films are not entirely amorphous but contain a small fraction of isolated nanocrystals, which contribute to a different extent to the film k value because their size is found to increase with increasing stack thickness. Consequently, it is inferred that the thermally induced crystallization of the as-grown amorphous LZO films is accompanied by a moderate k value enhancement also with respect to the parental ZrO_2 films.¹⁵ Given the connection between phonon vibrational spectra and k value,¹⁸ the above finding can be tentatively attributed to softening, through partial substitution of Zr with La atoms,¹⁹ of the c - or t - ZrO_2 infrared-active transverse optical phonon mode with minimum frequency.²⁰ Finally, it is ascertained from Fig. 4(c) that although RTA significantly degrades, compared to the as-grown state, the stack hardness to leakage paths, an acceptable leakage current density still flows through the MIS capacitor when pulsed in strong accumulation and inversion.

In conclusion, thin and uniform LZO films were grown on Si(100) by ALD at 300 °C using (¹PrCp)₃La, ZrD-04, and

O_3 . Their structural, chemical, and electrical properties were studied after 60 s vacuum annealing at 600 °C. Annealed films crystallize into a cubic or tetragonal ZrO_2 phases with a k value of ~ 30 . They are also immune to hygroscopicity and exhibit an acceptable leakage current density. Although such a high k value is desirable for EOT scaling down, process optimization is still required to minimize the sizable low- k silica-rich IL at the high- k /Si junction and (near) dielectric/Si interface defect density.

This work has been done as a part of the European FP6-Program “REALISE” (Grant No. IST-NMP 016172).

- ¹J. Robertson, *Rep. Prog. Phys.* **69**, 327 (2006).
- ²G. Scarel, A. Svane, and M. Fanciulli, in *Rare Earth Oxide Thin Films*, edited by M. Fanciulli and G. Scarel (Springer, Berlin, 2007), Vol. 106, Chap. 1, pp. 1–14.
- ³G. Scarel, A. Debernardi, D. Tsoutsou, S. Spiga, S. C. Capelli, L. Lamagna, S. N. Volkos, M. Alia, and M. Fanciulli, *Appl. Phys. Lett.* **91**, 102901 (2007).
- ⁴A. V. Prokofiev, A. I. Shelyakh, and B. T. Melekh, *J. Alloys Compd.* **242**, 41 (1996).
- ⁵Y. Zhao, M. Toyama, K. Kita, K. Kyuno, and A. Toriumi, *Appl. Phys. Lett.* **88**, 072904 (2006).
- ⁶M. C. Zeman, C. C. Fulton, G. Lucovsky, R. J. Nemanich, and W.-C. Yang, *J. Appl. Phys.* **99**, 023519 (2006).
- ⁷K. Bobzin, E. Lugscheider, and N. Bagcivan, *High Temp. Mater. Processes* **10**, 103 (2006).
- ⁸J. W. Seo, J. Fompeyrine, A. Guiller, G. Norga, C. Marchiori, H. Siegart, and J.-P. Locquet, *Appl. Phys. Lett.* **83**, 5211 (2003).
- ⁹J. Fompeyrine, G. Norga, A. Guiller, C. Marchiori, J. W. Seo, J.-P. Locquet, H. Siegart, D. Halley, and C. Rossel, *Proceedings of the WODIM 2002* (IMEP, Grenoble, France, 2002), p. 65.
- ¹⁰J. M. Gaskell, A. C. Jones, H. C. Aspinall, S. Taylor, P. Taechakumput, P. R. Chalker, P. N. Heys, and R. Odedra, *Appl. Phys. Lett.* **91**, 112912 (2007).
- ¹¹K. B. Jinesh, W. F. Besling, E. Tois, J. H. Klootwijk, W. Dekkers, M. Kaiser, F. Bakker, M. Tuominen, and F. Roozeboom, *Appl. Phys. Lett.* **93**, 062903 (2008).
- ¹²J. M. Gaskell, A. C. Jones, P. R. Chalker, M. Werner, H. C. Aspinall, S. Taylor, P. Taechakumput, and P. N. Heys, *Chem. Vap. Deposition* **13**, 684 (2007).
- ¹³R. L. Puurunen, *J. Appl. Phys.* **97**, 121301 (2005).
- ¹⁴G.-M. Rignanese, *J. Phys.: Condens. Matter* **17**, R357 (2005).
- ¹⁵A. Lamperti, L. Lamagna, G. Congedo, S. Spiga, and M. Fanciulli (unpublished).
- ¹⁶G. Katz, *J. Am. Ceram. Soc.* **54**, 531 (1971); G. Teufer, *Acta Crystallogr. Sect. A: Cryst. Phys., Diffr., Theor. Gen. Crystallogr.* **15**, 1187 (1962).
- ¹⁷A. Yoshigoe and Y. Teraoka, *Surf. Interface Anal.* **34**, 432 (2002).
- ¹⁸E. Bonera, G. Scarel, M. Fanciulli, P. Delugas, and V. Fiorentini, *Phys. Rev. Lett.* **94**, 027602 (2005).
- ¹⁹S. A. Shevlin, A. Curioni, and W. Andreoni, *Phys. Rev. Lett.* **94**, 146401 (2005).
- ²⁰X. Zhao and D. Vanderbilt, *Phys. Rev. B* **65**, 075105 (2002).
- ²¹W. A. Hill and C. C. Coleman, *Solid-State Electron.* **23**, 987 (1980).

TABLE I. Figures of merit for 13 nm as-grown and annealed LZO stacks (W =hysteresis width, V_{FB} =flatband voltage).

Stack state	W^a (mV)	V_{FB}^b (V)	D_{it}^c ($\times 10^{12} \text{ eV}^{-1} \text{ cm}^{-2}$)
as-grown	170(± 10)	-0.46(± 0.07)	3.8(± 0.4)
RTA in vacuum	40(± 10)	-1.47(± 0.15)	2.1(± 0.2)

^aReferenced to $C_{\text{max}}/2$ for a bidirectional $-2 \leftrightarrow +2$ V sweep at 100 kHz.

^bReferenced to the experimental 800 kHz C - V curve; theoretical value derived from the Al-Si work function difference is -0.21 V.

^cHill-Coleman method (Ref. 21) applied to the $G_p V$ peak at 100 kHz.